Free Energy Analysis of Cell Spreading

Eóin McEvoy
Department of Biomedical Engineering, National University of Ireland Galway
e.mcevoy5@nuigalway.ie

Vikram Deshpande
Department of Engineering, University of Cambridge, U.K.
vsd20@cam.ac.uk

Patrick McGarry (corresponding author)
Department of Biomedical Engineering, National University of Ireland Galway
Patrick.mcgarry@nuigalway.ie

ABSTRACT

In this study we present a steady-state adaptation of the thermodynamically motivated stress fiber (SF) model of Vigliotti *et al*. (2015). We implement this steady-state formulation in a non-local finite element setting where we also consider global conservation of the total number of cytoskeletal proteins within the cell, global conservation of the number of binding integrins on the cell membrane, and adhesion limiting ligand density on the substrate surface. We present a number of simulations of cell spreading in which we consider a limited subset of the possible deformed spread-states assumed by the cell in order to examine the hypothesis that free energy minimization drives the process of cell spreading. Simulations suggest that cell spreading can be viewed as a competition between (i) decreasing cytoskeletal free energy due to strain induced assembly of cytoskeletal proteins into contractile SF, and (ii) increasing elastic free energy due to stretching of the mechanically passive components of the cell. The computed minimum free energy spread area is shown to be lower for a cell on a compliant substrate than on a rigid substrate. Furthermore, a low substrate ligand density is found to limit cell spreading. The predicted dependence of cell spread area on substrate stiffness and ligand density is in agreement with the experiments of Engler *et al.* (2003). We also simulate the experiments of Théry *et al*. (2006), whereby initially circular cells deform and adhere to "V-shaped" and "Y-shaped" ligand patches. Analysis of a number of different spread states reveals that deformed configurations with the lowest free energy exhibit a SF distribution that corresponds to experimental observations, i.e. a high concentration of highly aligned SFs occurs along free edges, with lower SF concentrations in the interior of the cell. In summary, the results of this study suggest that cell spreading is driven by free energy minimization based on a competition between decreasing cytoskeletal free energy and increasing passive elastic free energy.

KEYWORDS

Cell Spreading, Thermodynamically Consistent Active Model, Cytoskeletal Free Energy, Cell Adhesion, Finite Element

ABBREVIATIONS

Stress fiber – SF; Focal adhesion – FA; Representative volume element – RVE

1. INTRODUCTION

Several experimental studies demonstrate that control of cell spreading using substrate micro-patterning has a significant impact on cell behavior. A study by McBeath *et al*. (2004) reveals that stem cell differentiation can be controlled by limiting cell spread area. It has also been shown that the contractility of smooth muscle cells increases with increasing cell area Tan *et al*. (2003). Lamers *et al*. (2010) show the spread geometry and stress fiber (SF) distribution of osteoblasts on grooved surfaces is highly dependent on groove spacing. Wide grooves result in polarized cells with SFs aligned along the grooves. Narrow groove spacing leads to randomly oriented cells and SFs. Finally, a study by Théry *et al*. (2006) has shown that when a cells spread on a "V-shaped" or "Y-shaped" ligand patch SFs align predominantly along the free edge of the cell and focal adhesions assemble along the perimeter of the ligand patch.

The bio-chemo-mechanical model proposed by Deshpande, *et al.* (2006) was used by McGarry *et al*. (2009) to analyze the aforementioned micro-post experiments of Tan *et al*. Simulations reveal that as cells spread the increasing number of adhered posts provide increasing support for SF tension and therefore reduce SF dissociation. Simulations also correctly predict that SFs are highly aligned along the free edges of the cell where the stress state is uniaxial. Using the same framework Pathak *et al*. (2008) analyzed the experiments of Théry *et al*. and, similar to McGarry *et al*., highly aligned stress fibers are predicted along the free edge of the cell. While these studies demonstrate the importance of tension support for stress fiber formation, they reveal a number of shortcomings of the phenomenological framework of Deshpande *et al.* (2006). Firstly, a high level of isotropic SF formation is incorrectly predicted to occur in regions of biaxial stress in the center of the cell. Experiments reveal that limited SF formation occurs in such regions. Secondly, the spread-state of the cell is assumed as the undeformed reference configuration. Clearly the cell deforms significantly from its spherical suspended state to reach the final spread-state.

In the current study we attempt to address these shortcomings by developing a steady-state finite element implementation of the recent thermodynamically motivated stress fiber model of Vigliotti *et al*. (2015). Our simulations of cells on micro-patterned substrates incorporate the following significant improvements on previous approaches: (i) The spread-state of the cell is not assumed as the strain free reference configuration. Rather, the cell deforms from a suspended geometry to reach its final spread configuration. The strain state of the deformed configuration is a key determinant of SF distribution in the cell. (ii) The number of cytoskeletal proteins in the cell is a finite and conserved quantity, requiring the development of a non-local numerical implementation. In contrast, McGarry *et al*. and Pathak *et al*. do not impose a global limit on SF formation. (iii) In addition to the advances presented in terms of our SF finite element model, we also propose a further development of the thermodynamically motivated focal adhesion assembly model of Deshpande *et al*. (2008) so that focal adhesion formation may be limited by a prescribed ligand density on the substrate to which a cell adheres.

An important consequence of the modelling approach is that there is not a unique final spread-state for the cell. Even in experiments such as those of Théry *et al*. and Tan *et al*. where the outline of the final spread shape is prescribed by micro-patterning ligand patches on the substrate, there is still an infinite number of ways in which the cell can spread across the patch geometry. Each final spread-state would have a different strain distribution and resultant SF distribution. Despite the infinite ways in which a cell can spread, the experimental heat maps of SF distribution in the study of Théry *et al*. reveal a strong trend of SF formation along free edges for a large number of cells. This suggests that the final spread state of a cell is not randomly generated. In this study we use our modelling framework to determine the free energy of the cell for a number of spread states and we hypothesize that cell spreading is driven by free energy minimization. Furthermore we ask if predicted SF and

focal adhesion distributions for minimum free energy spread states are in agreement with experimentally observed distributions.

This paper is structured as follows: In Section 2 we present our steady-state non-local stress fiber formation and cell spreading framework, followed by our model for ligand dependent focal adhesion assembly. We also introduce the factors contributing to the cell free energy. In Section 3 we consider a simplified example of axisymmetric spreading of a round cell on a flat substrate in order to demonstrate the key features of the computational framework and predict experimental trends observed by Engler *et al.* (2003). Finally, in Section 4 we simulate the experiments of Théry *et al*. by analyzing a number of spread-states for cells adhered to "V-shaped" and "Y-shaped" ligand patches.

2. MODELLING FRAMEWORK

2.1. Framework for Stress Fiber Remodeling and Contractility

The cytoskeleton is composed of actin-myosin stress fibers (SFs), which actively generate tension through cross-bridge cycling between the actin and myosin filaments. The thermodynamically consistent model from Vigliotti *et al*. (2015) captures key features of SF dynamics, including (i) The kinetics of stress fiber formation and dissociation as motivated by thermodynamic considerations, (ii) the stress, strain, and strain-rate dependence of SF remodeling, and (iii) global conservation of the cytoskeletal proteins. Here we implement a steady-state form of this continuum model in a two-dimensional finite element setting.

We envisage a two-dimensional (2D) cell of thickness b lying in the $x_1 - x_2$ plane (Figure 1a). A representative volume element (RVE) in the undeformed state is defined as a disk of radius $n^R l_0/2$. Stress fibers emanate from the center of this disk, each comprised of n^R functional units (of length l_0) in their initial ground state. In 2D plane stress SFs can form in

a large number of directions, with each direction defined by an angle ϕ with respect to the x_1-axis. At steady state, we consider that the (normalized) number of actin-myosin contractile units within a SF in direction ϕ in the RVE is given by:

$$\hat{n}(\phi) = \frac{n(\phi)}{n^R} = \big(1 + \varepsilon_n(\phi)\big)/(1 + \tilde{\varepsilon}_{ss}) \ \#(1)$$

where $\varepsilon_n(\phi)$ is the nominal strain in the direction ϕ. When a SF is extended, contractile units are added, with the effect that the internal strain in the SF is reduced until a steady state value $\tilde{\varepsilon}_{ss}$ is achieved (Figure 1b). $\tilde{\varepsilon}_{ss}$ is given by the positive root of the relation:

$$(p-1)\tilde{\varepsilon}_{ss}^{p} + p\tilde{\varepsilon}_{ss}^{p-1} - \frac{1}{\beta} = 0 \ \#(2)$$

where β and p are non-dimensional constants that govern the internal energy ψ of n^R functional units within a SF. Conversely, when a SF shortens, functional units are removed. In both cases, the internal fiber steady state strain $\tilde{\varepsilon}_{ss}$ is fixed and in general different from the axial material strain in the direction of the fiber, $\varepsilon_n(\phi)$.

2.1.1. Mass Conservation of Cytoskeletal Proteins

We assume spreading takes place during the interphase period of the cell cycle when the cell is in a homeostatic state (i.e. the concentration of all proteins within the cell is constant) (Weiss, 1996). Therefore, in the finite element framework developed in this study a global conservation of the total number of SF proteins N_0 within the entire cell is enforced. Cytoskeletal proteins are considered to exist in two states: a bound state and an unbound state. The bound proteins make up the functional units of the stress fibers within the RVE and thus are not mobile. The unbound proteins are mobile and can diffuse throughout the cell cytoplasm. The global conservation of cytoskeletal proteins may be expressed as

$$N_0 = N_u^{tot} + N_b^{tot} \ \#(3)$$

where N_u^{tot} and N_b^{tot} are the total numbers of unbound and bound cytoskeletal proteins in the entire cell. We next introduce the local normalized quantities: $\widehat{N}_u = N_u/N_0$, $\widehat{N}_b = N_b/N_0$, and $\widehat{N}_t = N_t/N_0$, where N_u and N_b are the local number of unbound and bound proteins within a given RVE, and the total number of proteins N_t locally in the RVE is obtained from

$$\widehat{N}_t = \widehat{N}_u + \widehat{N}_b \ \#(4)$$

Recall that the unbound proteins are mobile. Cytoskeletal proteins can diffuse through the cytoplasm at a rate of 1.5 $\mu m/s$ (McGrath et al., 1998) which is considered fast relative to the timescales of SF remodeling (Several studies report remodeling takes place over the course of hours (Kaunas et al., 2005; Wang et al., 2001)). Therefore it is reasonable to assume that for time-scales over which SFs remodel the total number of unbound proteins in the entire cell, N_u^{tot}, is uniformly distributed across all RVEs, i.e. $\widehat{N}_u$ is the same in all RVEs. Bound proteins, on the other hand, are not uniformly distributed throughout the cell, and $\widehat{N}_b$ in a given RVE must be computed from:

$$\widehat{N}_b = \int_{-\pi/2}^{+\pi/2} \hat{\eta}(\phi)\, \hat{n}(\phi)\, d\phi \ \#(5)$$

where $\eta(\phi)$ is the angular SF concentration per unit surface area of the RVE, with $\hat{\eta}(\phi) = \eta(\phi) n^R/N_0$. The global conservation condition (Equation 3) can therefore be expressed as:

$$\widehat{N}_u = 1. - \frac{1}{V_c}\int_{V_c} \widehat{N}_b\, dV \ \#(6)$$

where V_c is the total cell volume. In a numerical implementation, the global integral across the cell volume V_c in Equation 6 requires a non-local summation of $\widehat{N}_b$ across all integration points in the cell, as described in Section 2.1.5.

2.1.2. SF Angular Concentration and Active Stress Tensor

We next consider the kinetic equation for SF formation and dissociation proposed by Vigliotti *et al.*:

$$\dot{\hat{\eta}}(\phi) = \frac{\widehat{N}_u}{\pi \hat{n}(\phi)} \omega_n \exp\left[-\hat{n}(\phi)\frac{\mu_a - \mu_u}{kT}\right] - \hat{\eta}(\phi)\, \omega_n \exp\left[-\hat{n}(\phi)\frac{\mu_a - \mu_b(\phi)}{kT}\right] \#(7)$$

The first term on the right is the forward reaction rate for the formation of SFs, where ω_n is the molecular collision frequency of the SF proteins, k is the Boltzmann constant, T the absolute temperature, and μ_a is the activation enthalpy that must be surpassed for n^R proteins to form a SF. Here μ_u is the standard enthalpy of n^R unbound SF proteins, with $\mu_u = \mu_{u0} + \Delta\mu_{u0} C$. The unbound proteins are affected by an activation signal C and form more readily into their bound states as the signal (e.g. concentration of unfolded ROCK) increases, with μ_{u0} is the standard enthalpy of the unbound SF proteins in the absence of a signal ($C = 0$) and $\Delta\mu_{u0}$ the increase in the enthalpy of the unbound molecules at full signal activation ($C = 1$). At steady state we assume a continuous fully activated signal, i.e. $C = 1$. The second term on the right is the backward reaction rate for SF dissociation, with μ_b the standard enthalpy of n^R bound SF proteins, given as:

$$\mu_b \equiv \psi - \sigma_f(\phi)[1 + \varepsilon_n(\phi)]\Omega \#(8)$$

where Ω is the volume of n^R functional units in a SF in an undeformed RVE, and ψ is the internal energy of n^R functional units within a SF, given by:

$$\psi \equiv \mu_{b0} + \beta\mu_{b0}|\tilde{\varepsilon}_{ss}|^p \#(9)$$

where μ_{b0} is the internal energy of n^R functional units within a SF in their ground state, and $\sigma_f(\phi)$ is the tensile stress actively generated by a SF. In this paper we develop a steady state solution, hence Hill tension-velocity relationship does not need to be considered as $\sigma_f(\phi)$ is

necessarily equal to the maximum isometric tension σ_{max}. Here we consider steady state conditions so that $\dot{\hat{\eta}}(\phi) = 0$, therefore Equation 7 reduces to:

$$\hat{\eta}(\phi) = \frac{\hat{N}_u}{\pi \hat{n}(\phi)} \frac{\exp\left[-\hat{n}(\phi)\frac{\mu_a - \mu_u}{kT}\right]}{\exp\left[-\hat{n}(\phi)\frac{\mu_a - \mu_b(\phi)}{kT}\right]} \#(10)$$

and the normalized SF concentration in direction ϕ is given as:

$$\hat{\eta}(\phi) = \frac{\hat{N}_u}{\pi \hat{n}(\phi)} \exp\left[-\hat{n}(\phi)\frac{\mu_b(\phi) - \mu_u}{kT}\right] \#(11)$$

or from Equation 5:

$$\hat{\eta}(\phi) = \frac{\hat{N}_t - \int_{-\pi/2}^{+\pi/2} \hat{\eta}(\phi)\hat{n}(\phi)\, d\phi}{\pi \hat{n}(\phi)} B(\phi) \#(12)$$

where $B(\phi) = \exp[-\hat{n}(\phi)(\mu_b(\phi) - \mu_u)/kT]$, $\hat{N}_t$ is the total number of cytoskeletal proteins locally in an RVE, and the integral provides the total number of bound proteins in the RVE. Finally the 2D active stress tensor follows as:

$$\boldsymbol{\sigma}_{act} = \frac{\sigma_{max} f_0}{J} \int_{-\frac{\pi}{2}}^{\frac{\pi}{2}} \left(\hat{\eta}(\phi)[1 + \varepsilon_n(\phi)] \begin{bmatrix} cos^2\,\phi & \frac{sin\,2\phi}{2} \\ \frac{sin\,2\phi}{2} & sin^2\,\phi \end{bmatrix} \right) d\phi \#(13)$$

where f_0 is the volume fraction of cytoskeletal proteins in the cell, and J is the determinant of the deformation gradient $\boldsymbol{F}$.

2.1.3. Cytoskeletal Free Energy

The cytoskeletal free energy (g_{cyto}) is given as follows:

$$g_{cyto} = N_u^{tot} \chi_u + \int_{V_c} N_b\, \chi_b\, dV \#(14)$$

Where χ_u is the chemical potential of the unbound proteins that form a single SF functional unit, and χ_b is the chemical potential of a functional unit with a SF. From Equation 5:

$$g_{cyto} = N_u^{tot}\chi_u + \int_{V_c}\left(\int_{-\frac{\pi}{2}}^{\frac{\pi}{2}}\eta(\phi)\, n(\phi)\, d\phi\right)\chi_b\, dV \#(15)$$

As previously mentioned we assume infinitely fast diffusion of SF proteins and therefore a homogeneous distribution throughout the cell. Also Equation 10 implies thermodynamic equilibrium with $\chi_u = \chi_b$ which then simplifies Equation 15 to:

$$g_{cyto} = N_u^{tot}\chi_u + \chi_u \int_{V_c}\left(\int_{-\frac{\pi}{2}}^{\frac{\pi}{2}}\eta(\phi)\, n(\phi)\, d\phi\right)dV \#(16)$$

Here the double integral represents the total number of bound proteins in all RVEs in the cell. Therefore:

$$g_{cyto} = N_u^{tot}\chi_u + (N_0 - N_u^{tot})\,\chi_u = N_0\chi_u \#(17)$$

The chemical potential of the unbound proteins is $\chi_u = \mu_u + kT\ln(\widehat{N}_u)$ and thus:

$$g_{cyto} = N_0\left(\mu_u + kT\ln\left(\widehat{N}_u\right)\right)\#(18)$$

with the cytoskeletal energy per unit volume of the cell then given as

$$\bar{G}_{cyto} = \rho\left(\mu_u + kT\ln\left(\widehat{N}_u\right)\right)\#(19)$$

where $\rho \equiv N_0/V_c$ is the concentration of cytoskeletal proteins.

2.1.4. Passive Elasticity

The formulation is completed by the addition of a non-linear hyperelastic Ogden model (Ogden, 1972) in parallel with the SF model in order to represent the strain stiffening of the

mechanically passive cell components. As we consider the cell volume to remain constant during the analysis, the incompressible formulation is implemented:

$$\boldsymbol{\sigma}_{pas} = \sum_{i=1,2} \frac{2\mu}{\alpha} \left(\lambda_i^{\alpha} - (\lambda_1\lambda_2)^{-\alpha}\right) (\boldsymbol{m}_i \otimes \boldsymbol{m}_i) \#(20)$$

where μ is the material shear modulus, $\lambda_{1,2}$ are the principal stretches, $\boldsymbol{m}_{1,2}$ are the principal stretch directions, and α is a material constant. Here the passive elastic free energy per unit volume ($\bar{G}_{elas}$) is given by the Ogden strain energy density function:

$$\bar{G}_{elas} = \frac{2\mu}{\alpha^2} \left(\lambda_1^{\alpha} + \lambda_2^{\alpha} - (\lambda_1\lambda_2)^{-\alpha} - 3\right) \#(21)$$

The total Cauchy stress tensor at an integration point is obtained by summation of the passive and active contributions:

$$\boldsymbol{\sigma}_{Cauchy} = \boldsymbol{\sigma}_{pas} + \boldsymbol{\sigma}_{act} \#(22)$$

2.1.5. Numerical Implementation

In our numerical implementation we consider SF formation in a large number of discrete directions *M* (*M*=36 is found to provide a converged solution) in the 2D plane of each RVE in the cell. Equation 5 is approximated as

$$\widehat{N}_b = \frac{\pi}{M} \sum_{i=1}^{M} \hat{\eta}_i \hat{n}_i \quad \#(23)$$

where $\hat{\eta}(\phi_i)\hat{n}(\phi_i)$ is written in shorthand as $\hat{\eta}_i\hat{n}_i$. Equation 12 is therefore approximated as

$$\hat{\eta}_j \hat{n}_j \pi = B_j \widehat{N}_t - B_j \left(\frac{\pi}{M} \sum_{i=1}^{M} \hat{\eta}_i \hat{n}_i \right), \; j = 1, M \#(24)$$

Rearranging, we obtain

$$\hat{\eta}_j \hat{n}_j \left(\frac{1}{B_j}\right) - \left(\frac{1}{M}\sum_{i=1}^{M} \hat{\eta}_i \hat{n}_i\right) = \frac{\hat{N}_t}{\pi}, \quad j = 1, M \#(25)$$

or, in matrix form:

$$\begin{bmatrix} \left(\frac{1}{B_1}+\frac{1}{M}\right)\hat{n}_1 & \frac{1}{M}\hat{n}_2 & \dots & \frac{1}{M}\hat{n}_M \\ \frac{1}{M}\hat{n}_2 & \left(\frac{1}{B_2}+\frac{1}{M}\right)\hat{n}_2 & \dots & \frac{1}{M}\hat{n}_M \\ \dots & \dots & \dots & \dots \\ \frac{1}{M}\hat{n}_M & \frac{1}{M}\hat{n}_M & \dots & \left(\frac{1}{B_M}+\frac{1}{M}\right)\hat{n}_M \end{bmatrix} \begin{Bmatrix} \hat{\eta}_1 \\ \hat{\eta}_2 \\ \dots \\ \hat{\eta}_M \end{Bmatrix} = \frac{\hat{N}_t}{\pi} \begin{Bmatrix} 1 \\ 1 \\ \dots \\ 1 \end{Bmatrix} \#(26)$$

A solution for $\hat{\eta}_j$ (j=1,M) is obtained by matrix inversion. This steady-state model for SF formation and contractility is implemented via a *user-defined material* (UMAT) subroutine in the commercial finite element (FE) software package Abaqus. Prescribed boundary conditions are applied to the cell at the start of an analysis step, and contact conditions (see Section 2.2) with a substrate are enforced at cell nodes where appropriate. The solution is progressed through the analysis step, with each increment representing an iteration towards the final steady state solution. At each integration point the axial material nominal strains $\varepsilon_n(\phi)$ in each of the M stress fiber directions are determined from the material log strain tensor (STRAN), and number of functional units $\hat{n}(\phi)$ in each of the M directions is obtained from Equation 1. In the first increment of the analysis step it is assumed that all cytoskeletal proteins are unbound and uniformly distributed across all integration points in the cell mesh so that $\hat{N}_t = \hat{N}_u$. The solution for $\hat{\eta}(\phi)$ in M directions is obtained by inversion of the matrix on the left of Equation 26. The local Cauchy stress tensor $\boldsymbol{\sigma}$ is computed from Equations 13, 20, 22 and the consistent tangent matrix $\partial\Delta\boldsymbol{\sigma}/\partial\Delta\boldsymbol{\varepsilon}$ is approximated numerically based on a forward difference perturbation of the deformation gradient matrix (Sun *et al.* 2008), (Nolan et al., 2014), (Reynolds and McGarry, 2015)). At each integration point the local number of bound proteins $\hat{N}_b$ is calculated at the end of the increment, as per Equation 23. At the end of

an increment *i*, the total number of bound cytoskeletal proteins throughout the entire cell is computed through volume averaged summation of $\widehat{N}_b\big|^i$ across every integration point in the mesh in a *user-defined external database* (UEXTERNALDB) file, as outlined in Figure 2. In the subsequent increment the remaining available unbound proteins are redistributed so that a homogeneous distribution of $\widehat{N}_u\big|^{i+1}$unbound proteins is obtained in every RVE. The total number of proteins in the RVE is updated so that $\widehat{N}_t\big|^{i+1} = \widehat{N}_u\big|^{i+1} + \widehat{N}_b\big|^i$. Equation 26 is then solved and new values for $\hat{\eta}(\phi)|^{i+1}$, and thus $\boldsymbol{\sigma}|^{i+1}$ and $\widehat{N}_b\big|^{i+1}$ are obtained. Following the final increment of the analysis step the steady-state solution is achieved, and the cytoskeletal free energy $\bar{G}_{cyto}$ and elastic free energy $\bar{G}_{elas}$ are computed (Equations 19, 21).

2.2. Framework for Focal Adhesion Development

Binding integrins on the cell surface exist in two conformational states: a low affinity (bent) state or an active (straight) state with a high affinity to the appropriate ligand. Only high affinity integrins will bind to the substrate. Here we introduce an extension of the thermodynamic focal adhesion (FA) model from Deshpande *et al*. (2008), whereby we include a dependence of bond formation on ligand availability.

2.2.1. Focal Adhesion Model

We first define $\theta_L = C_L/N_L$ and $\theta_H = C_H/N_H$, with $\theta_L, \theta_H \leq 1$. Here C_L and C_H are the area densities of the unbound low affinity integrins and bound high affinity integrins, respectively, N_L is the area density of the unbound low affinity sites on the cell surface, and N_H is the area density of ligands on the substrate surface. The chemical potential of low affinity integrins at a density C_L is dependent on their internal energy and configurational entropy given by:

$$\chi_{\mathrm{L}} = \mu_L + kT \ln\left(\frac{\theta_L}{1-\theta_L}\right) \quad \#(27)$$

where μ_L is the enthalpy of the low affinity integrins, while k and T are the Boltzmann constant and absolute temperature. As only high affinity (or straight) integrins interact with substrate ligands, the high affinity chemical potential (at a density C_H) includes additional contributions due to the stretching of the bonds:

$$\chi_{\mathrm{H}} = \mu_H + kT \ln\left(\frac{\theta_H}{1-\theta_H}\right) + \Phi(\Delta_i) - F_i\Delta_i \quad \#(28)$$

where μ_H is the enthalpy of the high affinity integrins, $\Phi(\Delta_i)$ is the strain energy of the integrin-ligand complex, and the $-F_i\Delta_i$ term is the mechanical work that represents the loss in free energy due to the stretch Δ_i of the integrin-ligand (analogous to the pressure-volume term in the thermodynamics of gases), with:

$$F_i = \frac{\partial \Phi}{\partial \Delta_i} \#(29)$$

The stretch energy Φ is expressed as a piecewise quadratic potential:

$$\Phi = \begin{cases} \kappa_s\Delta_e^2 & \Delta_e \le \Delta_n \\ -\kappa_s\Delta_n^2 + 2\kappa_s\Delta_n\Delta_e - \kappa_s\Delta_e^2 & \Delta_n < \Delta_e \le 2\Delta_n \\ \kappa_s\Delta_n^2 & \Delta_e > 2\Delta_n \end{cases} \quad \#(30)$$

where κ_s is the stiffness of the integrin-ligand bond, $\Delta_e = \sqrt{\Delta_1 + \Delta_2}$ is the stretch magnitude, and Δ_n is the peak bond length. The bond stretch Δ_i is related to the displacement u_i of the cell membrane relative to the substrate as:

$$\Delta_i = \begin{cases} u_i & \Delta_e \le \Delta_n \ \ or \ \ \left[\frac{\partial \Phi}{\partial \Delta_e}\Delta_e < 0\right] \\ 0 & otherwise \end{cases} \#(31)$$

At thermodynamic equilibrium $\chi_H = \chi_L$, so Equations 27, 28 lead to:

$$\left(\frac{1-\theta_L}{\theta_L}\right)\left(\frac{\theta_H}{1-\theta_H}\right) = Z^* \#(32)$$

$$with\ Z^* = \exp\left(\frac{\mu_L - \mu_H - \Phi(\Delta_i) + F_i\Delta_i}{kT}\right) \#(33)$$

which gives the local area densities of low and high affinity integrins. Similar to the SF model, we implement global conservation of integrins on the cell surface:

$$S_0C_0 = S_0(1-\delta)N_L^0\theta_L + \int_{S_a}\left[N_L\,\theta_L + \frac{N_H\,Z^*\,\theta_L}{(1-\theta_L) + Z^*\,\theta_L}\right]dS \#(34)$$

where S_0 is the undeformed reference surface area of the cell, and C_0 is the initial density of integrins on the cell surface. The term on the left S_0C_0 is a conserved value, giving the total number of integrins on the cell surface. S_a is the surface area in contact with the substrate, δ is the fraction of the cell adhered to the substrate, and N_L^0 is the initial undeformed area density of low affinity binding sites on the cell surface. The first term on the right gives the total number of low affinity integrins on the unadhered cell surface, while the second term gives the total number of integrins (high and low affinity) on the adhered cell surface. The local tractions on the cell surface are depend on the concentration of bound high affinity integrins and the force on each ligand-integrin complex, and are balanced by the stresses in the cell:

$$T_i = \sigma_{ij}n_{ij} = -C_HF_i \#(35)$$

Where σ_{ij} is the Cauchy stress in the cell, and n_{ij} is the surface normal.

2.2.2. Focal Adhesion Free Energy

The adhesion free energy is given by:

$$g_{adh} = \int_{S_a}(C_L\,\chi_L + C_H\,\chi_H)\,dS \#(36)$$

However at thermodynamic equilibrium $\chi_H = \chi_L, so$:

$$g_{adh} = \chi_L \, S_0 \, C_0 \#(37)$$

with the adhesion energy per unit cell volume given as

$$\bar{G}_{adh} = \frac{\chi_L \, S_0 \, C_0}{b \, S_0} \#(38)$$

where b is the cell thickness in its undeformed configuration. Then, $\bar{G}_{adh}$ follows as:

$$\bar{G}_{adh} = \frac{C_0}{b}\left(\mu_L + kT \ln\left(\frac{\theta_L}{1-\theta_L}\right)\right) \#(39)$$

2.2.3. Numerical Implementation

The focal adhesions between the cell and the micro-patterned substrates are included in the analysis through a *user-defined interface* (UINTER) subroutine in Abaqus. Adhesions can develop at any node on the cell surface that comes in contact with the substrate, dependent on the local tractions and availability of integrins. At each node θ_L is recorded at the end of the increment, as per Equation 32. Recall that the area density of low affinity integrins $C_L = \theta_L N_L$. At the end of an increment *i,* the global area density of low affinity integrins on the cell surface is computed through area averaged summation of $\theta_L|^i$ across every node on the surface in a *user-defined external database* (UEXTERNALDB) file (Figure 2). Mass conservation of integrins is enforced by Equation 34. In the subsequent increment the remaining available unbound low affinity integrins are redistributed so that a homogeneous distribution of $\theta_L|^{i+1}$ is obtained across the surface. We assume the time-scales associated with integrin diffusion are fast relative to the time-scales of focal adhesion assembly. Efficient achievement of a converged solution the UINTER requires the specification of an accurate stiffness matrix. An exact analytical solution is obtained from:

$$\frac{\partial T_i^A}{\partial u_j} = -\left[C_H \frac{\partial F_i}{\partial u_j} + F_i \frac{\partial C_H}{\partial u_j}\right] \#(40)$$

We make the assumption that the substrate is infinitely stiff relative to the cell, and therefore has a negligible free energy.

2.3. Material Parameters

All simulations are reported for cells at a temperature $T = 310K$. The parameters for the SF framework are fixed at those used in Vigliotti *et al*. (2015) with the volume fraction $f_0 = 0.032,\ \Omega = 10^{-7.1}\mu m^3,\ \beta = 1.2,\ p = 2,\ \tilde{\varepsilon}_{ss} = 0.35,$ and the maximum isometric tension $\sigma_{max} = 240\ kPa$ (Lucas et al., 1987). In keeping with the parameter studies of Vigliotti *et al.* $(\mu_{u0} + \Delta\mu_{u0}) = 8\ kT,\ \mu_{b0} = 9\ kT$. The density of cytoskeletal proteins in the cell ρ is $2\ x10^6\ \mu m^{-3}$, calibrated such that the cytoskeletal free energy is competitive with the passive free energy. The passive elastic parameters are $\mu = 1.66\ kPa$ and $\alpha = 8$, determined through simulation of the Engler *et al*. (2003) experiments for cells spreading on substrates of increasing stiffness. For the FA model, parameters were constrained to lie within commonly accepted ranges as per Deshpande *et al*. (2008). The total area density of integrins C_0 is 5000 μm^{-2} (Lauffenburger and Linderman, 1993), the bond stiffness $\kappa_s = 0.15\ nN\ \mu m^{-1}$, and the maximum allowable stretch in the bond $\Delta_n = 50\ nm$, such that the surface energy $\bar{\gamma} = \kappa_s \Delta_n^2 / kT$ is in the upper end of the range reported by Leckband and Israelachvili (2001). The difference in the reference chemical potentials for the low and high affinity integrins is taken as $\mu_H - \mu_L = 5kT$ (McCleverty and Liddington 2003). The model was extended to allow for dependence on the number of available ligands and non-local conservation of integrins. A parametric study was performed to determine an appropriate ligand density to ensure sufficient adhesions could form, taken to be $N_H = 25\ X\ 10^3 \mu m^{-2}$. The availability of binding sites should always be greater than the maximum number of bound high affinity

integrins, taken here as $N_L = 50\ X\ 10^3 \mu m^{-2}$. A summary of key parameters is provided in Table 1.

3. 2D ANALYSIS OF CELL SPREADING ON INFINITE FLAT SUBSTRATES

We illustrate the features of the modelling framework by considering the axisymmetric spreading of a round cell on flat substrates under plane stress conditions, as shown in Figure 3. Material incompressibility is assumed. Solutions are presented for both a rigid and a compliant substrate. Additionally the solutions are presented for both a high and low substrate ligand density. In the undeformed configuration the cell has a radius r and thickness b. Cell spreading is simulated in two analysis steps: (i) Displacement ("pre-stretch") boundary conditions are applied to the cell so that its radius is increased to λr with a uniform strain state throughout; (ii) Contact is implemented between the deformed cell and the substrate and the displacement boundary condition is removed. Surface and integrin-ligand attachments are formed in accordance with Equations 27-35. The active cell stress tensor is computed from Equation 13 and is added to the passive stress tensor (Equation 22). In addition to deformation of the cell and integrin-ligand attachments, the substrate will also deform due to the passive and active cell stress (except in cases where the substrates can be considered to be infinitely stiff compared to the cell). This finite element scheme determines the steady state configuration of the cell, adhesions, and substrate. For a given steady state configuration the total free energy density of the system is computed from

$$\bar{G}_{tot} = \bar{G}_{cyto} + \bar{G}_{elas} + \bar{G}_{adh} + \bar{G}_{sub} \quad \#(41)$$

Analyses are performed for a range of "pre-stretch" (λ) values and the free energy density of the system is plotted as a function of the steady-state spread area of the cell. As stated in Section 1, we hypothesize that a cell tends towards a spread-state that reduces the free energy of the system.

Results: We first consider the case of cell spreading on a rigid substrate. The force generation by the actin-myosin machinery lowers the chemical potential of the stress fiber proteins in the bound state and thereby favoring the formation of stress fibers. As the cell stretches to its spread configuration, functional units are added to the stress fiber chain in order to reduce the internal SF strain ($\tilde{\varepsilon}_n$) to the ground state (dictated by $\tilde{\varepsilon}_{ss}$). Thereby an increase in cell spreading results in a decrease in $\widehat{N}_u$ (Figure 4a), and consequently the free energy of the cytoskeletal proteins ($\bar{G}_{cyto}$) is lowered (Figure 4b). However as shown in Figure 4c, an increase in spreading also results in an increase in the elastic free energy of the cell due to straining of the passive (hyperelastic) non-contractile components of the cell. This framework therefore presents cell spreading as a competition between a decrease in cytoskeletal free energy due to strain induced stress fiber formation and an increase in elastic free energy due to straining of the passive cell components. As illustrated in Figure 4e, for the limited number of spread states considered here, a low free energy configuration is computed at an area of $A/A_0 \approx 2.75$. Any further spreading beyond this point will incur a significant elastic penalty due to the strain stiffening hyperelastic passive component of the model. Our computed low free energy spread area corresponds closely to the experimental observations of Engler et al. (2003), where cell spread areas on rigid substrates are approximately three times higher than unspread cell areas.

In the case of cell spreading on a compliant substrate, an increase in cell spread area incurs an elastic penalty (increasing free energy) from both the passive elastic components of the cell and the elastically deformed substrate. These elastic penalties are plotted in Figures 5c and 5e for cell spreading on a compliant neo-Hookean substrate ($\mu = 8$kPa), and once again are in direct competition with the reducing cytoskeletal free energy (Figure 5b) as the cell spreads. When $A/A_0 < 1$ the cell has contracted below the reference area due to substrate

deformation. In such cases $\bar{G}_{elas}$ increases due to compression of the passive cell components. The lowest free energy configuration on this compliant substrate is computed at a spread area of $A/A_0 \approx 1.8$ (Figure 5f). This spread area is 30% lower than the low energy spread area on a rigid substrate (Figure 4e). Once again, this result corresponds closely to the experimental study of Engler *et al.* (2003) where the cell spread areas of on 8kPa substrates are observed to be ~25% lower than on rigid substrates. This further supports our hypothesis that the cell will tend towards a spread state that reduces its free energy.

Figure 4d and 5d demonstrate that cell spreading also results in increased focal adhesion formation, with a consequent reduction in the adhesion free energy. The change in adhesion free energy over the range of spread configurations is ~3 orders of magnitude lower than the cell cytoskeletal and elastic free energies. Therefore focal adhesion formation does not significantly contribute to the energetic competition that governs cell spreading in Figures 4 and 5. However, cell spreading is not possible without a sufficient degree of traction mediated focal adhesion assembly, as mechanical equilibrium of the spread cell is only achieved by traction interaction with the substrate. An increase in traction results in an increase in the density of high affinity integrins (C_H). As the cell spreads, the tractions between the cell and substrate increase (due to both elastic stretching of passive components and higher contractility due to increased strain induced SF formation), and consequently C_H increases. The entropy of integrins on the cell surface increases as more integrins are in a bound state (in accordance with Equation 39). Therefore, an increase in C_H during spreading results in a decrease in $\bar{G}_{adh}$, as shown in Figure 4d. A higher ligand density will inherently allow the cell to spread further as higher cellular tractions can be supported by the focal adhesions. In contrast, Figure 6 considers the case of a rigid substrate with a low ligand density ($N_H = 2500\ \mu m^{-2}$), which limits the cell spreading. The final spread area increases with the initially applied cell pre-stretch up to a value of $\lambda \approx 1.5$. If the cell is initially

stretched beyond this point, a sufficient number of integrin-ligand bonds cannot be formed to support the resultant tractions, and the cell shrinks to a steady-state area of $A/A_0 \approx 1.85$. This is the maximum spread area that the cell can reach for this low ligand density. Note that if the cell cannot adhere to the substrate (e.g. ligand density of zero), an unadhered cell is predicted to shrink to an area of A/A_0=0.735 and a total free energy density of $\hat{\bar{G}}_{tot} = 5.65$ is observed. As shown in Figure 6b, the total free energy reduces with increasing spread area, but spread states with $A/A_0 \geq 1.85$ cannot occur due to the low ligand density. Recall from Figure 4e that a high ligand density $N_H = 25000\ \mu m^{-2}$ results in a low free energy spread area of $A/A_0 = 2.75$ (also shown in Figure 6a for comparison). Our predicted ~33% reduction in cell spread area for a 10-fold decrease in ligand density is again supported by the experimental results of Engler *et al*. (2003).

4. 2D ANALYSIS OF CIRCULAR CELL SPREADING ON MICRO-PATTERNED SUBSTRATES

We next attempt to simulate the experiments of Théry *et al*. (2006) whereby cells are spread on micro-patterned ligand patches under plane stress conditions. Two patch geometries are considered: "V-shaped" patches, and "Y-shaped" patches, as shown in Figure 7. For simplicity we assume that the cell is initially circular with radius r_c when in suspension. It is important to note that there is an infinite number of spread states (strain distributions) that can be assumed by the cell in order to spread on the ligand patch. Here we attempt to parameterize the spreading process by considering a subset of possible spread states. In the case of the "V-shaped" patch the cell is stretched so that proportion of the cell perimeter ωr_c can adhere to the outer edge of the "V". The stretch is assumed to be uniform along the patch and is given as $\lambda_c = L_s/\omega r_c$, where L_s is the fixed patch length. Therefore, by considering a

range of values of λ_c (or ω) we can simulate a number of spread states and determine which of these states produces the lowest total free energy. The cell radius in the initial configuration is $r_c = 17\ \mu m$ and the thickness $b = 1\ \mu m$. The substrate dimensions are based on the experiments of Théry *et al*. (2006), i.e. $L_s = 46\mu m$ and the substrate letter width was determined to be $7\mu m$. Once again the total steady state free energy density is computed from Equation 41.

Results: Similar to the simplified axisymmetric example presented in Section 4, the cell free energy during spreading can be interpreted as a competition between the increasing elastic free energy ($\bar{G}_{elas}$) and the decreasing cytoskeletal free energy ($\bar{G}_{cyto}$). Simulations of cell spread on a V-shaped substrate reveal that $\bar{G}_{tot}$ is minimized at a cell perimeter stretch of $\lambda_c = 1.3$ (Figure 8a). Examination of the strain distribution in this lowest free energy (LFE) configuration (Figure 8b) reveals that the maximum tensile strain occurs close to the free unadhered edge of the spread cell. A spread state characterized by a lower stretch ($\lambda_c = 1.1$) results in an elevated total free energy $\bar{G}_{tot}$, despite a high concentration of straight SFs directly along the free edge. Such a configuration results in extremely high strains along the free unadhered edge, causing a very high elastic free energy penalty. A spread state characterized by a higher stretch ($\lambda_c = 1.6$) results in a high strain in the region of the adhered edges. Although this allows more a similar level of SF formation on all three edges of the spread cell (Figure 8c), the high elastic penalty due to stretching along the adhered edges is too large to be compensated for by the reduction in $\bar{G}_{cyto}$ due to SF formation along all three edges. The density of bound SF proteins is characterized by $\zeta^{SF}(\phi) = \hat{n}(\phi) * \hat{\eta}(\phi)$, with Figure 8c showing the dominant SF orientation at each material point. The focal adhesion distribution in these highlighted configurations (Figure 8c) show evident clustering in the direction of traction, denoted by $\hat{C}_H = C_H/N_H$. However, the variance in $\bar{G}_{adh}$ between these configurations was negligible.

Figure 9 shows the dominant SF alignment (d) and FA distribution (c) in the LFE configuration for cells spread on the V-shaped substrate. We see that the highest SF concentration and actin density (ζ^{SF}) is in the region of the free edge where an arc of SFs curve towards the center of the cell. A similar distribution is reported in the experimentally determined heat maps of SF distribution reported by Théry *et al.* (Figure 9b). At the center of the cell, where the strain is lowest in both cases, Equation 12 dictates that the SF concentration in any direction will be lower than that along the free edge. Focal adhesions ($\hat{\mathrm{C}}_{\mathrm{H}}$) are predicted to form along the perimeter of the ligand patch due to a shear-lag type distribution of traction between the cell and the patch. Such a FA distribution is also reported in the experimental study of Théry *et al*. (2006) (Figure 9a).

Simulations of cell spread on a Y-shaped substrate reveal that $\bar{G}_{tot}$ is minimized at a perimeter stretch of $\lambda_c = 1.34$ (Figure 10a) on two of the free edges, with a slightly higher strain and SF concentration on the third (top) edge. Once again a spread state characterized by a higher or lower value of λ_c results in an elevated $\bar{G}_{tot}$ due to an extremely high elastic free energy.

The experimental SF heat maps for the Y-patterned substrate from Théry *et al*. (2006) exhibit an expected symmetry, with similar SF patterns on all three free edges. However, in the computed LFE configuration (Figure 10) one edge has a higher strain and SF concentration. In order to compare our computational results to an experimental heat map (constructed using data from several observations) we should acknowledge that there are three LFE configurations due to symmetry of the Y-shape. Therefore we rotate the distributions shown in Figure 10c-d through 120^{o} and 240^{o} we then construct a "computational heat map" by taking the average of these three LFE distributions. The "computational heat map" is shown

in Figure 11c-d and exhibits an identical SF distribution on all three free edges and can be directly compared to the experimental heat maps. Notably the "computational heat map" free edge SF concentration is lower than that along the free edge of the V-shape (Figure 9d) ("heat map averaging" is not necessary for the V-shape as it has only one free edge). This prediction is supported by experimental results (Figures 9b and 11b).

5. DISCUSSION

In this paper we present a steady-state adaptation of the thermodynamically motivated continuum SF model of Vigliotti *et al*. (2015). We implement this formulation in a non-local finite element setting where we consider global conservation of the total number of cytoskeletal proteins within the cell, global conservation of the number of binding integrins on the cell membrane, and a finite ligand density on the substrate surface.

When a number of cytoskeletal proteins assemble to form contractile SFs, the free energy of the proteins bound within the SF is lower than the total free energy of the same proteins when they are unbound (not assembled in a SF). During spreading the strain in a cell increases. This results in assembly of cytoskeletal proteins into contractile SFs, and a consequent lowering of the total cytoskeletal free energy in the cell. Of course an increase in cell strain during spreading also results in an increase in the elastic free energy of the mechanically passive components of the cell (e.g. the membrane, intermediate filaments etc.). Therefore cell spreading can be viewed as a competition between the reducing cytoskeletal free energy and the increasing elastic free energy. Our analyses suggest that the driver of cell spreading is a lowering (or perhaps a minimization) of the total free energy of the system.

To simulate cell-substrate contact we present an extension of the Deshpande *et al*. (2008) model for FA kinematics, whereby we account for a dependence on the substrate ligand

density. Variance of the substrate ligand density has significant impact on cell behaviour. Combined with the mass conservation of integrins, this affects the maximum cellular tractions the FAs can withstand, and therefore the spread shape and area.

In Section 3 the key features of the model are examined through a series of simplified simulations of axisymmetric cell spreading. By considering a number of parameterized cell spread states on a rigid substrate our analyses suggest that the lowest free energy spread-state has an area that is 2.75 times higher than an unspread cell area. This prediction is in agreement with the experimental measurements of Engler et al. (2003). Furthermore, when cells spread on compliant substrates ($\mu = 8$kPa) we predict that the lowest free energy spread area is ~30% lower than the corresponding area on a rigid substrate. Once again this finding is supported by the experimental trends reported in Engler et al. (2003). Finally, we predict that a low substrate ligand density will limit the spread area of a cell, with a 10-fold decrease in ligand density on a rigid substrate resulting in a ~33% reduction in spread area on a rigid substrate. Again, this prediction is in broad agreement with the experimental measurements of Engler et al. (2003) and Gaudet et al. (2003). Our hypothesis that cell spreading is driven by a lowering of free energy appears to provide an explanation for the broad trends observed by Engler et al. (2003).

A recent study by Shenoy *et al. (2016)* suggests that the cellular free energy decreases with increasing substrate stiffness, which provides an energetic basis for durotaxis. The results from Section 3 of the current study also provides insight to this phenomenon. In the lowest energy spread configuration on a compliant substrate, the cell has a predicted free energy of $\widehat{\overline{G}}_{tot} = 4.85$. However, on a rigid substrate the lowest free energy configuration is observed at $\widehat{\overline{G}}_{tot} = 4.2$. Therefore, we suggest that durotaxis is the result of a cell attempting to lower its free energy by migrating towards a stiffer substrate. Similarly, chemotaxis may be explained

by the inability of a cell to attain a minimum free energy configuration if the concentration of ligands is very low, thus inducing the cell to migrate to a region of higher ligand density in order to reduce the free energy.

In Section 4 a number of parameterized spread-states are simulated, whereby a circular cell adheres to "V-shaped" and "Y-shaped" ligand patches based on the experiments of Théry *et al*. (2006). The free energy associated with each spread state is computed, and we demonstrate that the spread-state with the lower free energy exhibits a SF distribution that corresponds to experimental observations, i.e. a high concentration of highly aligned SFs occurs along free edges, with lower SF concentrations at the interior of the cell. The simulation of the complex SF and FA distributions observed experimentally in cells spread on the V- and Y- shaped ligand patterns demonstrates the predictive power of the model. Future implementations will also consider cell spreading on grooves (Lamers et al. 2010) and micro-posts (McGarry et al. 2009; Ronan et al. 2013). The current analysis presents a movement away from traditional deterministic approaches to computational cell biomechanics in which the experimentally observed spread state is incorrectly assumed to be the reference undeformed state. Such approaches neglect cell strain as a driver of SF assembly. Also, global conservation of a finite number of cytoskeletal proteins within the cell has been neglected. The model of Pathak *et al*. (2008) simulates the experiments of Théry *et al*. (2006) using such assumptions. The degree of SF alignment (characterized by a variance parameter) is correctly predicted, with uniaxial SFs being predicted in a region of uniaxial stress along the cell free edge (in accordance with the model of Deshpande *et al*. (2006) SFs orthogonal to the free edge dissociate due to the stress-free condition). However, the framework incorrectly predicts full SF formation in all directions (isotropic distribution) in areas of biaxial stress and in regions where the cell is bonded to the ligand patch. The current

study corrects such shortcomings by considering strain associated with cell spreading, in addition to implementing a global conservation of cytoskeletal proteins.

In this study we consider a very small subset* of the possible spread-states of a cell on a micro-patterned substrate, in order to examine the dependence of the SF distribution on the manner in which a cell spreads (*our subset is primarily chosen based on ease of parameterization, as illustrated in Figure 7, rather than on any consideration of the actual cell spreading process). Our analysis of a number of spread states allows us to examine the hypothesis that the final spread state is driven by minimization of the free energy of the system. In reality however, there are an infinite number of spread configurations that the cell can assume. A rigorous treatment of the stochastic problem of cell spreading requires the development of a statistical mechanics framework that allows for the analysis of an extremely large number of spread states. The finite element framework developed here is prohibitively computationally expensive for such an approach.

The underlying premise in this work is that minimum/low free-energy configurations are the most likely states to be observed. In statistical thermodynamics a closed system in a constant temperature and pressure environment attains equilibrium at minimum Gibbs free-energy. However, a cell is not a closed system and in fact never attains an equilibrium state in this sense while alive. The approach taken here of searching for low free-energy states rests on the "homeostatic ensemble" developed by Shishvan et al. (2017) who show that in their homeostatic state cells attain a fluctuating equilibrium where low free-energy states are more probable. The results presented here should be viewed in this light, in the sense that the minimum free-energy configurations predicted in our analyses have the highest probability of being observed in experiments.

6. CONCLUDING REMARKS

We combine the thermodynamically consistent model for the stress fiber cytoskeleton developed by Vigliotti *et al*. (2015) with a focal adhesion model (again motivated by thermodynamic considerations) to analyze two problems: (i) spreading of cells on elastic substrates and (ii) spreading of cells on substrates with specific geometrical ligand patterns.

Spreading of cells is shown to be a competition mainly between the elastic energy and cytoskeletal energy of the cell, as well as the elastic energy of the substrate. With increasing cell spreading the elastic energy of the cell and substrate typically increases, but the cytoskeletal energy decreases as a larger fraction of the cytoskeletal proteins form stress fibers. The equilibrium configuration is assumed to be that corresponding to the lowest free energy. In agreement with the experiments of Engler et al. (2003) we show that the spread area of the cell increases with increasing substrate stiffness. When the spreading of cells is constrained by specific geometric patterns of ligands, we show that, in the lowest free-energy configuration, stress fibers preferentially form along the un-adhered edges of the cell, in line with the observations of Théry *et al*. (2006). This framework presents a potential computational tool to design substrates and scaffolds that will yield a desired cell spread state.

The simulations presented here suggest that computed low (or minimum) free-energy spread cell configurations are broadly consistent with experimentally observed spread cell configurations. However, it is worth emphasizing that cells do not attain an equilibrium minimum free-energy configuration in the traditional sense, as observations clearly show that spread cells are in a perpetually fluctuating state. Thus, the minimum free-energy configuration is best viewed as the most probable state to be observed, rather than a unique equilibrium state.

APPENDIX A

The influence of an applied steady-state nominal strain ε_n on the steady-state active and passive Cauchy stress is illustrated in Figure A1(a) (material parameters as per Section 2.3) for a cell subjected to series of uniaxial stretches. The dependence of stress fiber formation (Equation 12) on steady-state strain (Figure A1(b)) is reflected in the strain dependence of the active stress (through Equation 13). It must be noted that the active stress curve in Figure A1(a) is not representative of a stress-strain constitutive law. Rather, it is a plot of the steady-state active stress computed for an applied steady-state strain. In contrast, previous modelling approaches (e.g. Deshpande *et al* 2006) do not include a dependence of stress fiber formation on applied strain, so that the computed stress fiber activation-level (SFA) and, consequently, the active stress are independent of the applied steady state strain in Figure A1.

ACKNOWLEDGMENT

Funding support was provided by the Irish Research Council (IRC) postgraduate scholarship (GOIPG/2015/2954), the National University of Ireland Galway Hardiman scholarship, and Science Foundation Ireland (SFI-12/IP/1723). The authors would like to acknowledge the Irish Centre for High-End Computing (ICHEC) for provision of computational facilities and support.

REFERENCES

Deshpande, V.S., McMeeking, R.M., Evans, A.G., 2006. A bio-chemo-mechanical model for cell contractility. Proc. Natl. Acad. Sci. U. S. A. 103, 14015–20. doi:10.1073/pnas.0605837103

Deshpande, V.S., Mrksich, M., McMeeking, R.M., Evans, A.G., 2008. A bio-mechanical model for coupling cell contractility with focal adhesion formation. J. Mech. Phys. Solids 56, 1484–1510. doi:10.1016/j.jmps.2007.08.006

Engler, A., Sheehan, M., Sweeney, H.L., Discher, D.E., 2003. Substrate compliance vs ligand density in cell on gel responses. Eur. Cells Mater. 6, 7–8. doi:10.1016/S0006-3495(04)74140-5

Gaudet, C., Marganski, W. a, Kim, S., Brown, C.T., Gunderia, V., Dembo, M., Wong, J.Y., 2003. Influence of type I collagen surface density on fibroblast spreading, motility, and contractility. Biophys. J. 85, 3329–3335. doi:10.1016/S0006-3495(03)74752-3

Kaunas, R., Nguyen, P., Usami, S., Chien, S., 2005. From The Cover: Cooperative effects of Rho and mechanical stretch on stress fiber organization. Proc. Natl. Acad. Sci. 102, 15895–15900. doi:10.1073/pnas.0506041102

Lamers, E., Frank Walboomers, X., Domanski, M., te Riet, J., van Delft, F.C.M.J.M., Luttge, R., Winnubst, L.A.J.A., Gardeniers, H.J.G.E., Jansen, J.A., 2010. The influence of nanoscale grooved substrates on osteoblast behavior and extracellular matrix deposition. Biomaterials 31, 3307–3316. doi:10.1016/j.biomaterials.2010.01.034

Lauffenburger, D.A., Linderman, J.J., 1993. Receptors : models for binding, trafficking, and signaling. Oxford University Press.

Leckband, D., Israelachvili, J., 2001. Intermolecular forces in biology. Q. Rev. Biophys. 34, 105–267.

Lucas, S.M., Ruff, R.L., Binder, M.D., 1987. Specific tension measurements in single soleus and medial gastrocnemius muscle fibers of the cat. Exp. Neurol. 95, 142–54.

McBeath, R., Pirone, D.M., Nelson, C.M., Bhadriraju, K., Chen, C.S., 2004. Cell Shape,

Cytoskeletal Tension, and RhoA Regulate Stem Cell Lineage Commitment. Dev. Cell 6, 483–495. doi:10.1016/S1534-5807(04)00075-9

McCLEVERTY, C.J., LIDDINGTON, R.C., 2003. Engineered allosteric mutants of the integrin alphaMbeta2 I domain: structural and functional studies. Biochem. J. 372.

McGarry, J.P., Fu, J., Yang, M.T., Chen, C.S., McMeeking, R.M., Evans, a G., Deshpande, V.S., 2009. Simulation of the contractile response of cells on an array of micro-posts. Philos. Trans. A. Math. Phys. Eng. Sci. 367, 3477–3497. doi:10.1098/rsta.2009.0097

McGrath, J.L., Tardy, Y., Dewey, C.F., Meister, J.J., Hartwig, J.H., 1998. Simultaneous Measurements of Actin Filament Turnover, Filament Fraction, and Monomer Diffusion in Endothelial Cells. Biophys. J. 75, 2070–2078. doi:10.1016/S0006-3495(98)77649-0

Nolan, D.R., Gower, A.L., Destrade, M., Ogden, R.W., McGarry, J.P., 2014. A robust anisotropic hyperelastic formulation for the modelling of soft tissue. J. Mech. Behav. Biomed. Mater. 39, 48–60. doi:10.1016/j.jmbbm.2014.06.016

Ogden, R.W., 1972. Large Deformation Isotropic Elasticity - On the Correlation of Theory and Experiment for Incompressible Rubberlike Solids. Proc. R. Soc. London A Math. Phys. Eng. Sci. 326.

Pathak, A., Deshpande, V.S., McMeeking, R.M., Evans, A.G., 2008. The simulation of stress fiber and focal adhesion development in cells on patterned substrates. J. R. Soc. Interface 5, 507–524. doi:10.1098/rsif.2007.1182

Reynolds, N.H., McGarry, J.P., 2015. Single cell active force generation under dynamic loading - Part II: Active modelling insights. Acta Biomater. 27, 251–263. doi:10.1016/j.actbio.2015.09.004

Ronan, W., Pathak, A., Deshpande, V.S., McMeeking, R.M., McGarry, J.P., 2013.

Simulation of the mechanical response of cells on micropost substrates. J. Biomech. Eng. 135, 1–10. doi:10.1115/1.4025114

Shenoy, V.B., Wang, H., Wang, X., 2016. A chemo-mechanical free-energy-based approach to model durotaxis and extracellular stiffness-dependent contraction and polarization of cells. Interface Focus 6, 20150067. doi:10.1098/rsfs.2015.0067

Shishvan, S.S., Vigliotti, A., and V.S. Deshpande., 2017. The homeostatic ensemble for cells. (*Submitted)*

Sun, W., Chaikof, E.L., Levenston, M.E., 2008. Numerical approximation of tangent moduli for finite element implementations of nonlinear hyperelastic material models. J. Biomech. Eng. 130, 61003. doi:10.1115/1.2979872

Tan, J.L., Tien, J., Pirone, D.M., Gray, D.S., Bhadriraju, K., Chen, C.S., 2003. Cells lying on a bed of microneedles: An approach to isolate mechanical force. Proc. Natl. Acad. Sci. 100, 1484–1489. doi:10.1073/pnas.0235407100

Théry, M., Pépin, A., Dressaire, E., Chen, Y., Bornens, M., 2006. Cell distribution of stress fibers in response to the geometry of the adhesive environment. Cell Motil. Cytoskeleton 63, 341–355. doi:10.1002/cm.20126

Vigliotti, A., Ronan, W., Baaijens, F.P.T., Deshpande, V.S., 2015. A thermodynamically motivated model for stress-fiber reorganization. Biomech. Model. Mechanobiol. doi:10.1007/s10237-015-0722-9

Wang, J.H., Goldschmidt-Clermont, P., Wille, J., Yin, F.C., 2001. Specificity of endothelial cell reorientation in response to cyclic mechanical stretching. J. Biomech. 34, 1563–72.

Weiss, T.F., 1996. Cellular Biophysics (Vol. 1). MIT Press.

FIGURE CAPTIONS

Figure 1*:* a) *Schematic of a 2D cell on a ligand-coated substrate with the coordinate system marked. The networks of stress fibers and focal adhesions within the 2D RVE are shown in the inset; b) Remodeling of a SF subjected to a nominal tensile strain ε_n: (i) SF in ground state, with functional unit strain $\tilde{\varepsilon}_n = 0$; (ii) SF subjected to tensile strain ε_n which reduces the actin-myosin overlap; (iii) Remodeling of SF by addition of functional unit; (iv) Remodeled SF now in low energy state, with functional unit strain $\tilde{\varepsilon}_n = \tilde{\varepsilon}_{ss}$. (Vigliotti et al.,2015)*

Suggested Size: 1.5 column

Figure 2*: Outline of solution scheme. Total steady state energy density $\bar{G}_{tot}$ is calculated at the end of the analysis through the use of a UEXTERNALDB subroutine.*

Suggested Size: 1.5 column

Figure 3*: Axisymmetric cell spread schematic. A cell of radius r stretches over an infinite ligand patterned substrate.*

Suggested Size: 2 column

Figure 4*: For a rigid substrate, the relationship between cellular spread area and (a) the number of available unbound cytoskeletal proteins ($\hat{N}_u$), (b) the cytoskeletal free energy ($\bar{G}_{cyto}$), (c) the elastic free energy ($\bar{G}_{elas}$), (d) the adhesion free energy ($\bar{G}_{adh}$), and (e) the combined total free energy density ($\bar{G}_{tot}$). Free energy densities characterized by normalized quantity $\hat{\bar{G}} = \bar{G}/\rho kT$.*

Suggested Size: 2 column

Figure 5*: For a compliant neo-Hookean substrate ($\mu = 8kPa$), the relationship between cellular spread area and (a) the number of available unbound cytoskeletal proteins ($\hat{N}_u$), (b) the cytoskeletal free energy ($\bar{G}_{cyto}$), (c) the elastic free energy ($\bar{G}_{elas}$), (d) the adhesion free energy ($\bar{G}_{adh}$), (e) the substrate free energy ($\bar{G}_{sub}$), and (f) the combined total free energy density ($\bar{G}_{tot}$). Free energy densities characterized by normalized quantity $\hat{\bar{G}} = \bar{G}/\rho kT$.*

Suggested Size: 2 column

Figure 6*: (a) Steady state cell spread area as a function of applied cell "pre-stretch" λ for a low and high ligand density N_H (μm^{-2}) on a rigid substrate. The spread area with the lowest free energy (from Figure 4e) is marked by the grey circle. (b) The relationship between cell spread area and the total free energy ($\bar{G}_{tot}$) for a low ligand density ($N_H = 2500\,\mu m^{-2}$). Free energy densities characterized by normalized quantity $\hat{\bar{G}} = \bar{G}/\rho kT$.*

Suggested Size: 1.5 column

Figure 7*: Parametric study schematic of cell spreading on a) V- and b) Y- shaped substrates. For a cell of radius r_c, the spreading process is parameterized in terms of the proportion of the cell perimeter ωr_c that stretches along the ligand coated patch ($\lambda_c = L_s/\omega r_c$). The shaded patch represents locations focal adhesions may form with the cell surface.*

Suggested Size: 2 column

***Figure 8**: Predicted steady-state cell spread on V-shaped ligand pattern in a series of configurations: a) Free energy of the system ($\hat{\bar{G}}_{tot} = \bar{G}_{tot}/\rho kT$) for a range of spread states characterized by the stretch of the cell on the fixed edge (λ_c). Three states are highlighted: 1. A large stretch on the unadhered edge ($\lambda_c = 1.1$); 2. The lowest free energy configuration ($\lambda_c = 1.3$); 3. A large stretch on the adhered edge ($\lambda_c = 1.6$); b) Maximum principal strain (ε_p^{max}) distribution in the spread cell in the highlighted states; c) Distribution of vinculin or focal adhesions characterized by normalized quantity $\hat{C}_H = C_H/N_H$, and the dominant SF alignment in the highlighted configurations with $\zeta^{SF}(\phi) = \hat{n}(\phi) * \hat{\eta}(\phi)$.*

Suggested Size: 2 column

***Figure 9**: Cell spread on V-shaped micro-patterned substrates: Experimental images of average (a) vinculin and (b) actin distributions (Reproduced with some modifications from Théry et al. (2006). Copyright © John Wiley & Sons, Ltd.); (c) Distribution of vinculin or focal adhesions in the LFE configuration, characterized by normalized quantity $\hat{C}_H = C_H/N_H$; (d) Dominant SF alignment in the LFE configuration, with $\zeta^{SF}(\phi) = \hat{n}(\phi) * \hat{\eta}(\phi)$. The insets show full SF distribution for all M discrete directions.*

Suggested Size: 1.5 column

***Figure 10**: Predicted steady-state cell spread on Y-shaped ligand pattern in a low free energy configuration: a) Free energy of the system ($\hat{\bar{G}}_{tot} = \bar{G}_{tot}/\rho kT$) for a range of spread states characterized by the stretch of the cell on the fixed edge (λ_c). A lowest free energy (LFE) configuration is observed at $\lambda_c = 1.34$; b) Maximum principal strain distribution in the spread cell; c) Distribution of vinculin or focal adhesions in the LFE configuration, characterized by normalized quantity $\hat{C}_H = C_H/N_H$ d) Dominant SF alignment in the LFE configuration, with $\zeta^{SF}(\phi) = \hat{n}(\phi)\hat{\eta}(\phi)$. The insets show full SF distribution for all M discrete directions.*

Suggested Size: 1.5 column

***Figure 11**: Cell spread on Y-shaped micro-patterned substrates: Experimental images of average vinculin (a) and actin (b) distributions (Reproduced with some modifications from Théry et al. (2006). Copyright © John Wiley & Sons, Ltd.); (c) Predicted average distribution of vinculin or focal adhesions, characterized by normalized quantity $\hat{C}_H = C_H/N_H$; (d) Predicted average actin distribution, with $\zeta^{SF}(\phi) = \hat{n}(\phi) * \hat{\eta}(\phi)$.*

Suggested Size: 1.5 column

For appendix:

***Figure A1**. (a) Computed active steady state stress as a function of applied steady state nominal strain ε_n for the current model (active(1)). The passive and total stresses are also shown. For comparison the active stress computed by the Deshpande et al. (2006) model (active(2)) is shown. (b) Computed values of $\hat{\eta}$ as a function of applied steady state nominal strain ε_n for the current model. For comparison the stress fiber activation (SFA) level computed by the Deshpande et al. (2006) model is plotted to highlight the absence of strain dependence on SF remodeling in this previous model.*

Suggested Size: 1 column

Parameter symbol	Brief description
$n;\ n^R$	Number of functional units in a stress fiber; reference number of functional units within stress fiber in an undeformed RVE
η	Angular concentration of stress fibers at orientation (ϕ)
Ω	Volume of n^R functional units of the stress fiber
l_0	Undeformed length of a functional unit
$\varepsilon_n; \tilde{\varepsilon}_{ss}$	Nominal strain of a stress fiber; functional unit strain at steady state
$N_b; N_u$	Number of cytoskeletal proteins bound in functional units; number of unbound cytoskeletal proteins
$\mu_a; \mu_u; \mu_b$	Activation enthalpy for n^R cytoskeletal proteins; enthalpy of n^R cytoskeletal proteins in the unbound state; enthalpy of n^R cytoskeletal proteins in bound state
$\mu_{u0}; \mu_{b0}$	Standard enthalpy of n^R functional units in the unbound and bound states
ψ	Internal energy of n^R functional units within a stress-fiber
$\sigma_f; \sigma_{max}$	Stress fiber stress; maximum tensile stress of a stress-fiber
$f_0; \rho$	Volume fraction of cytoskeletal proteins in the cell; concentration of cytoskeletal proteins
$\chi_u; \chi_b$	Chemical potential of the unbound cytoskeletal proteins that form a single functional unit; chemical potential of a functional unit within a stress fiber
$C_0; C_L; C_H$	Initial area density of integrins on the cell surface; area densities of the unbound low affinity integrins and bound high affinity integrins
$S_0; S_a$	Undeformed reference surface area of the cell; surface area in contact with substrate
$N_L; N_H$	Area density of the unbound low affinity sites on the cell surface; Area density of ligands on the substrate surface
$\theta_L; \theta_H$	C_L / N_L; C_H / N_H
$\mu_L; \mu_H$	Enthalpy of the low affinity integrins; enthalpy of the high affinity integrins
Φ	Strain energy of the integrin-ligand complex
$\Delta_i; \Delta_n$	Stretch of the integrin-ligand complex; peak bond length
κ_s	Stiffness of the integrin-ligand complex
$\chi_L; \chi_H$	Chemical potential of low affinity integrins; chemical potential of high affinity integrins
$\bar{G}_{tot};\ \bar{G}_{cyto};\ \bar{G}_{elas};\ \bar{G}_{adh};\ \bar{G}_{sub}$	Total, cytoskeletal, elastic, adhesion, and substrate free energy densities

***Table 1**: A summary of key parameters of the model*

rev_fig1.tif

Click here to download high resolution image

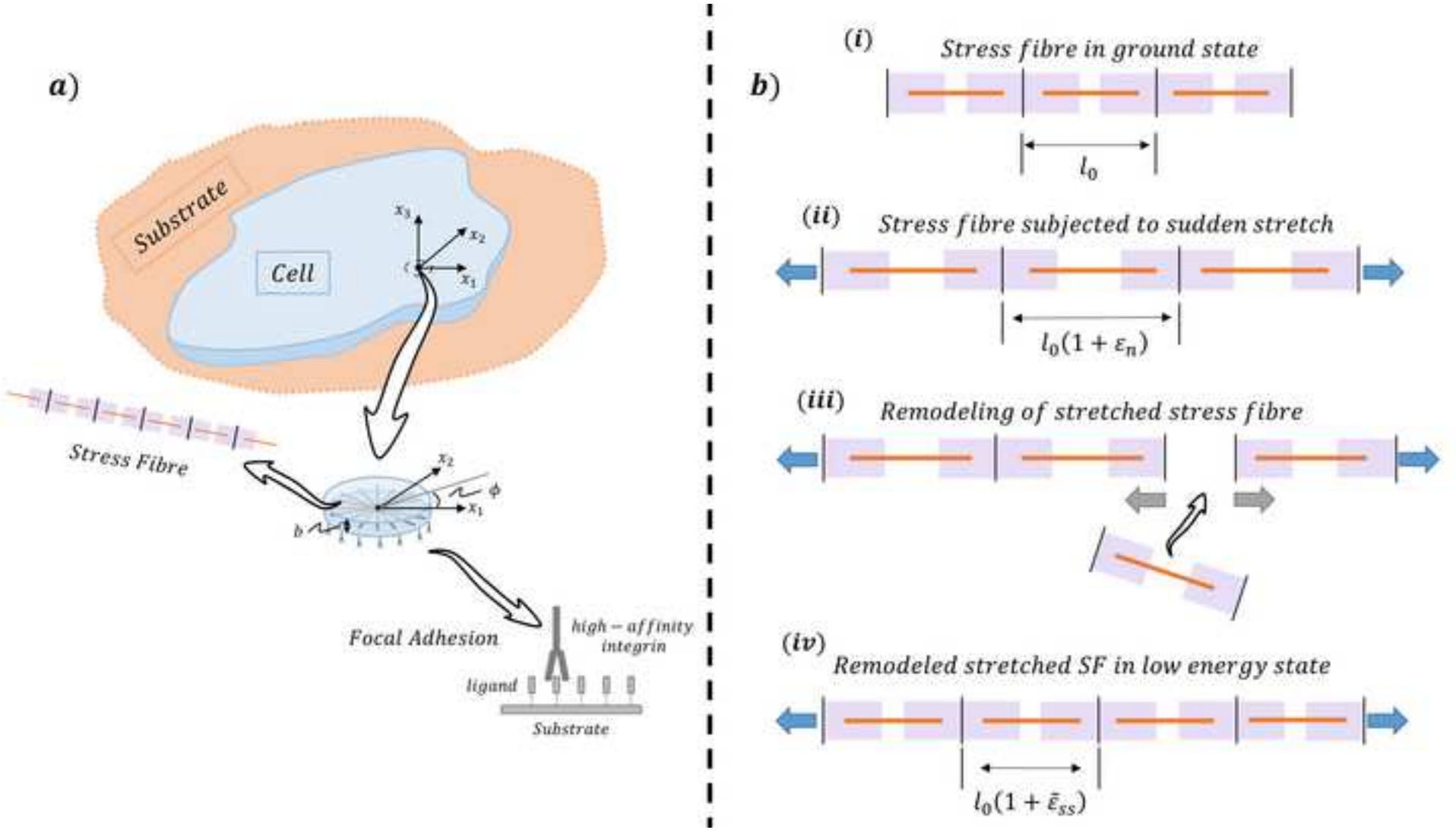

rev_fig2.tif
Click here to download high resolution image

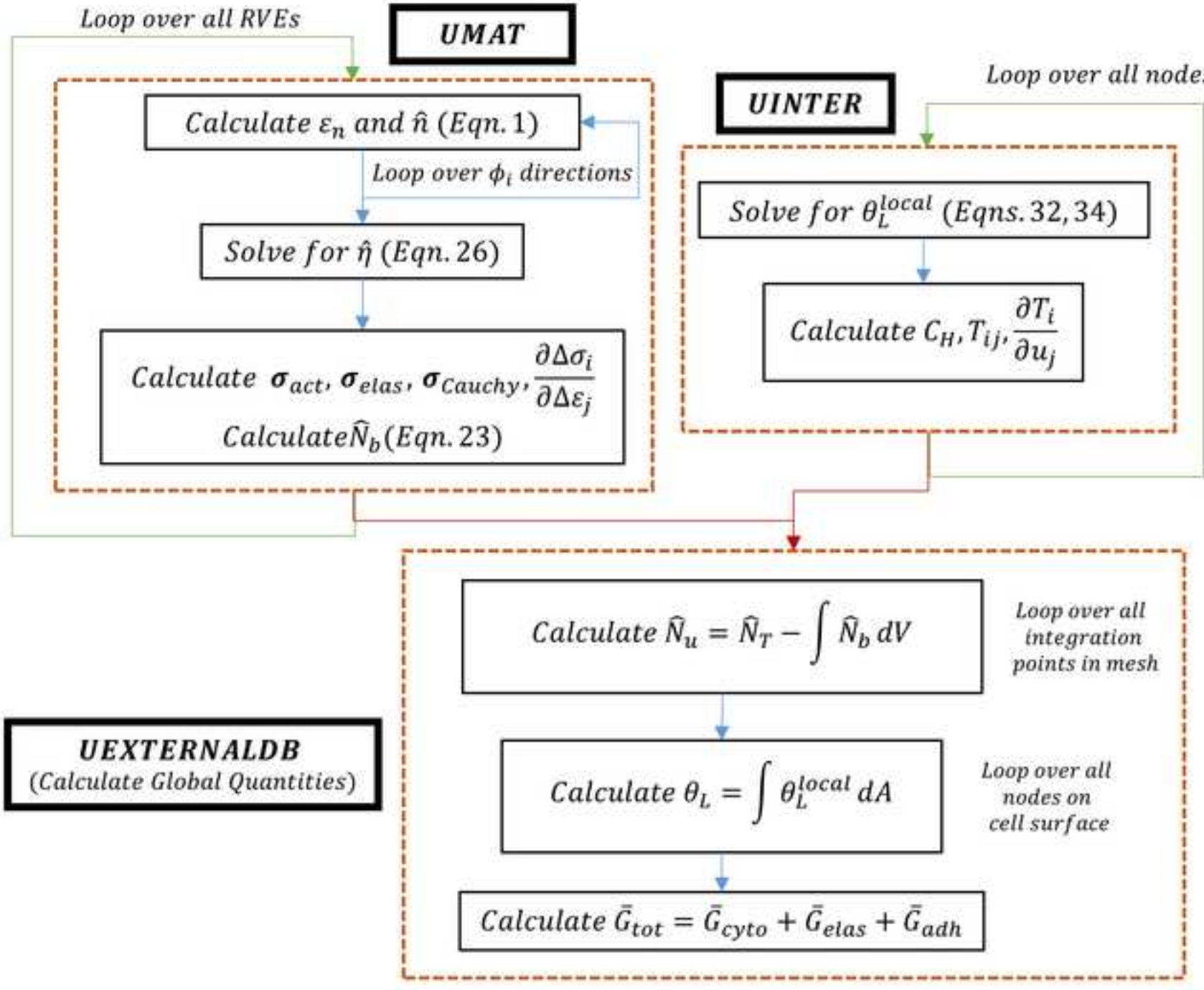

rev_fig3.tif
Click here to download high resolution image

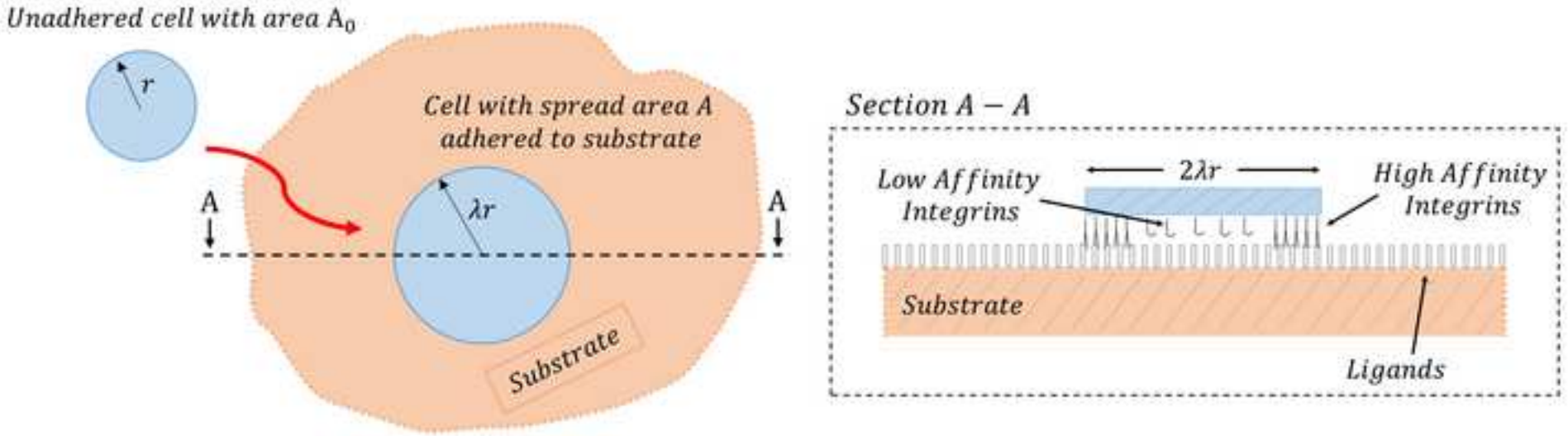

rev_fig4.tif

Click here to download high resolution image

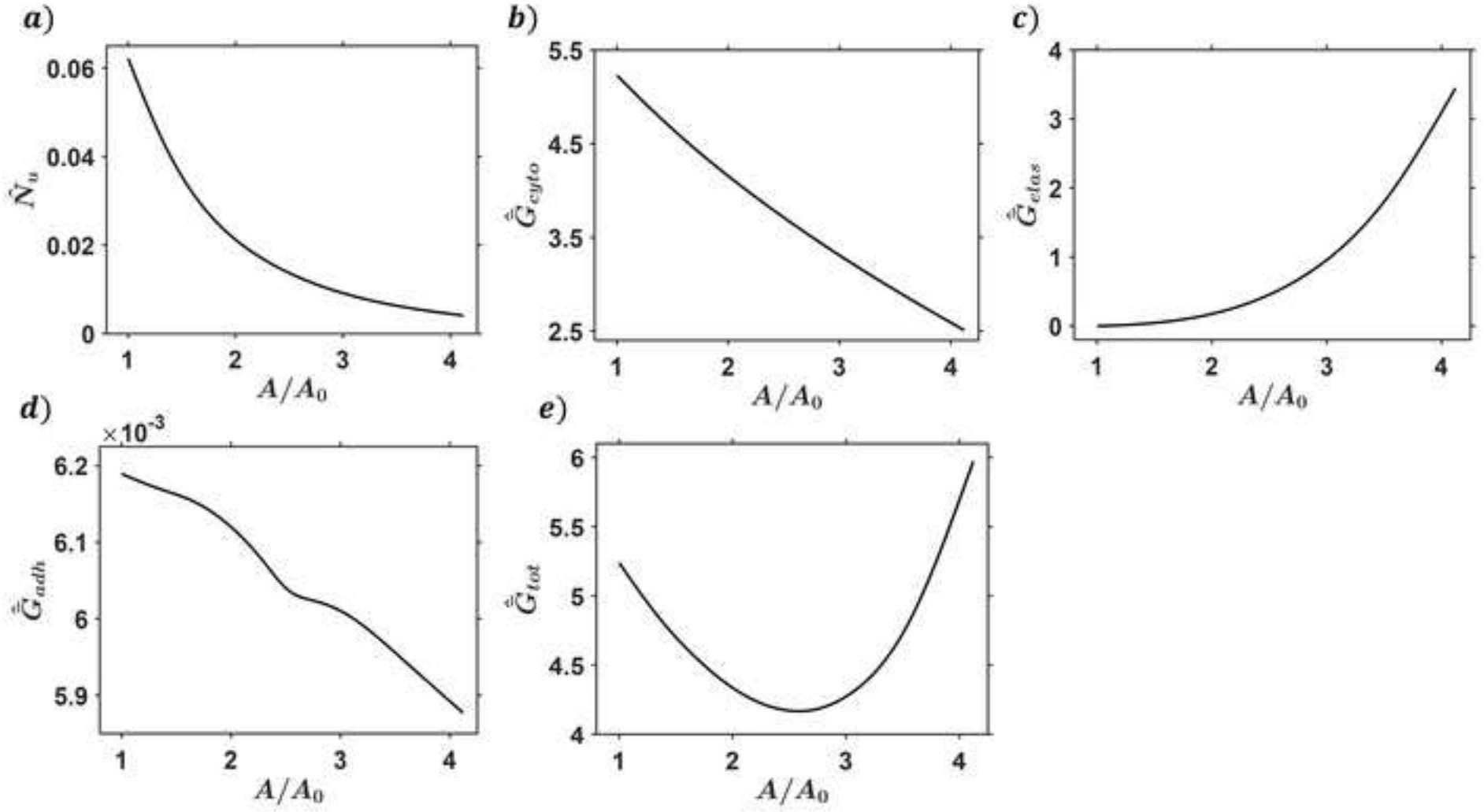

rev_fig5.tif

Click here to download high resolution image

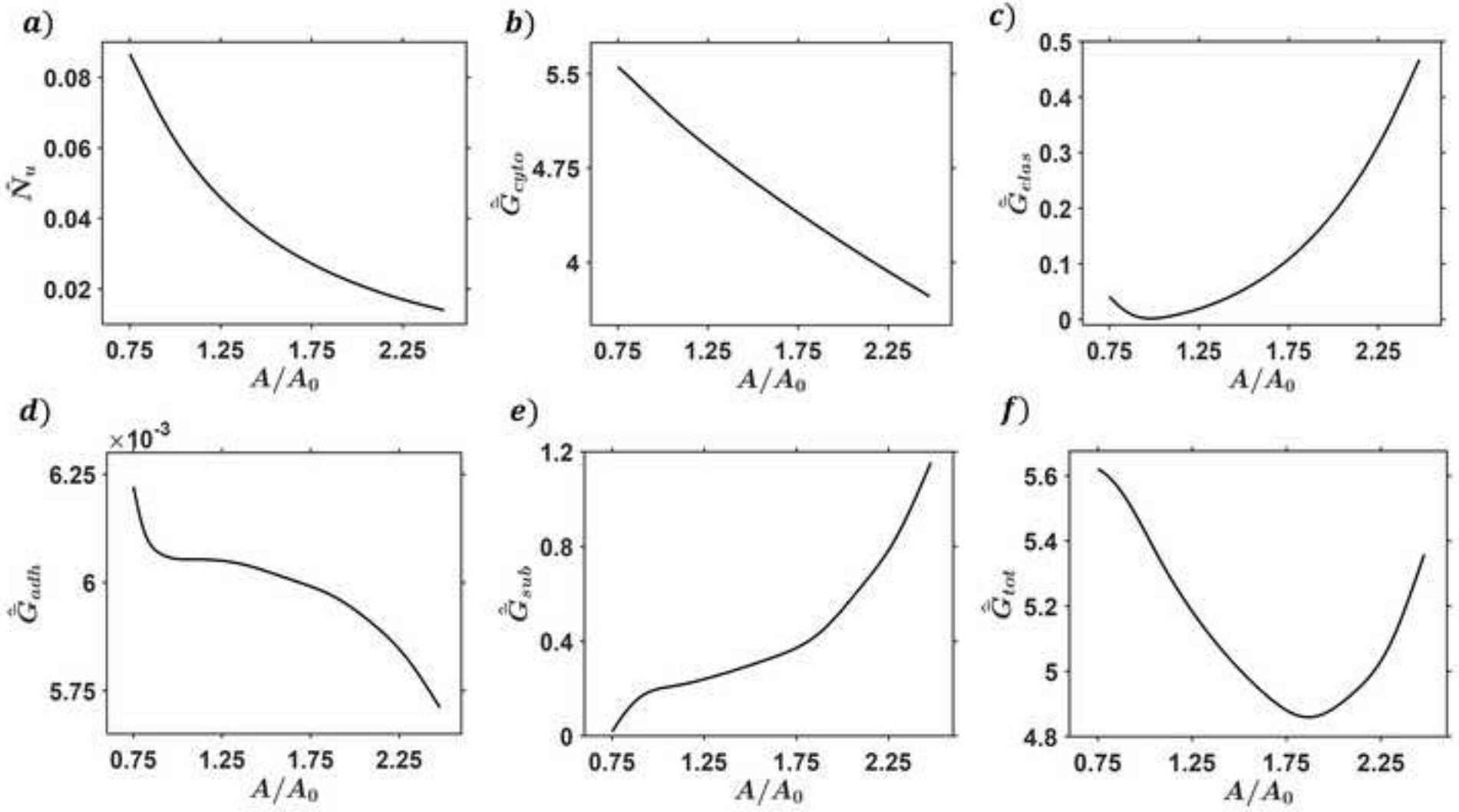

rev_fig6.tif
Click here to download high resolution image

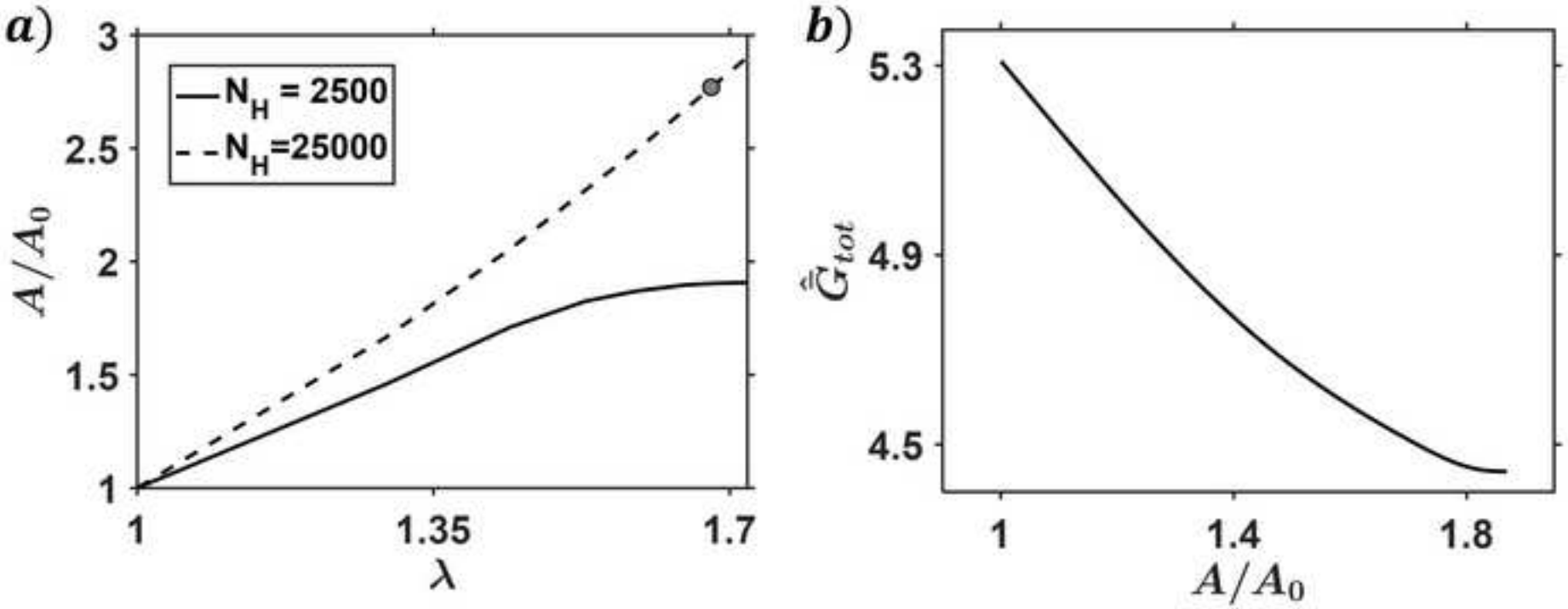

rev_fig7.tif
Click here to download high resolution image

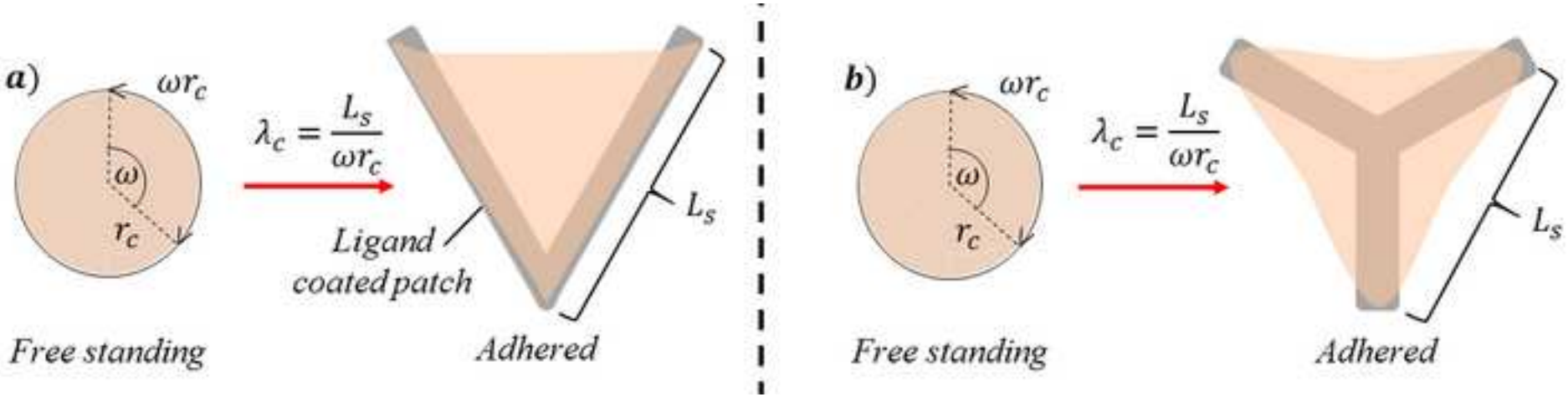

rev_fig8.tif

Click here to download high resolution image

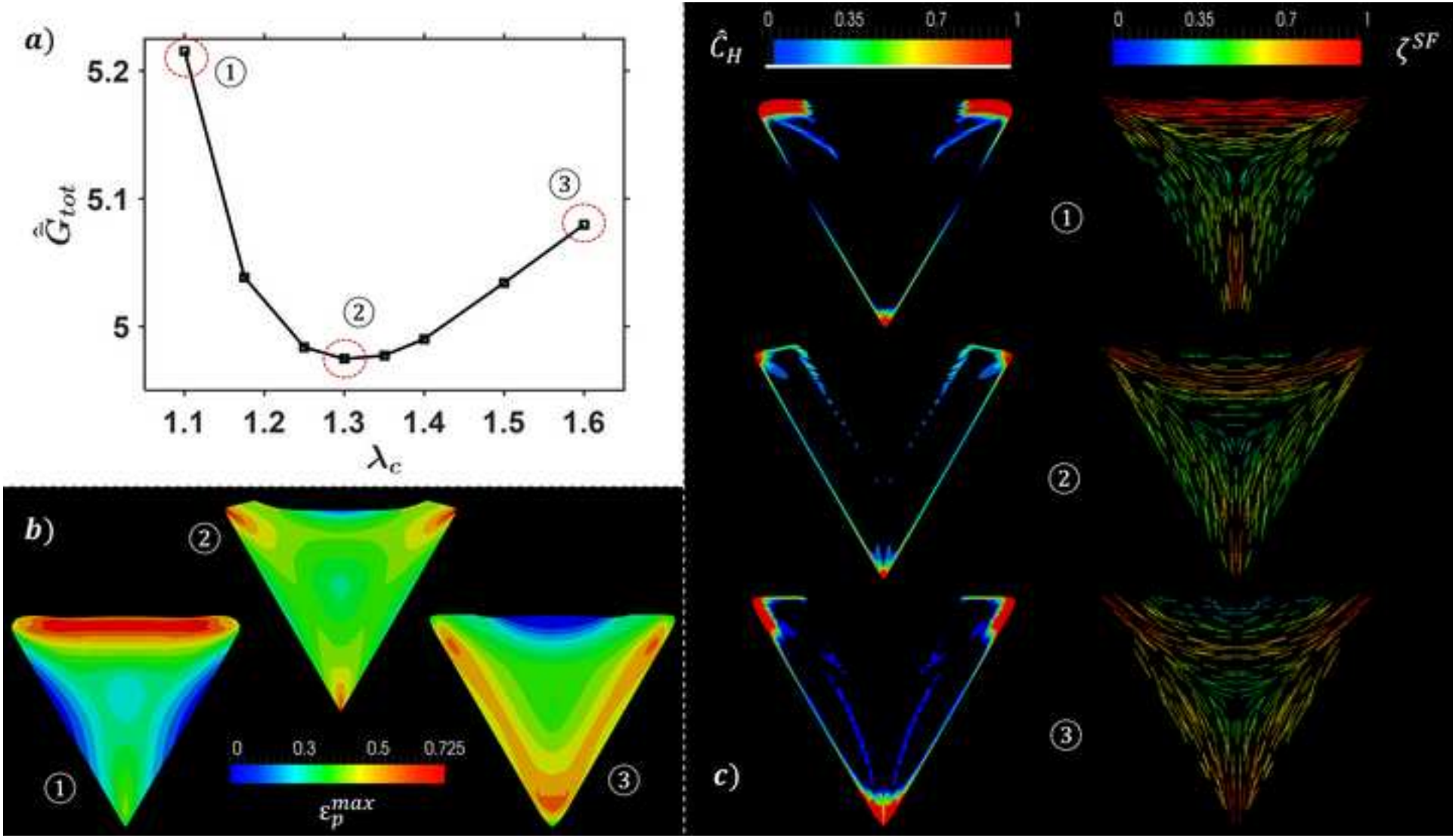

rev_fig9.tif
Click here to download high resolution image

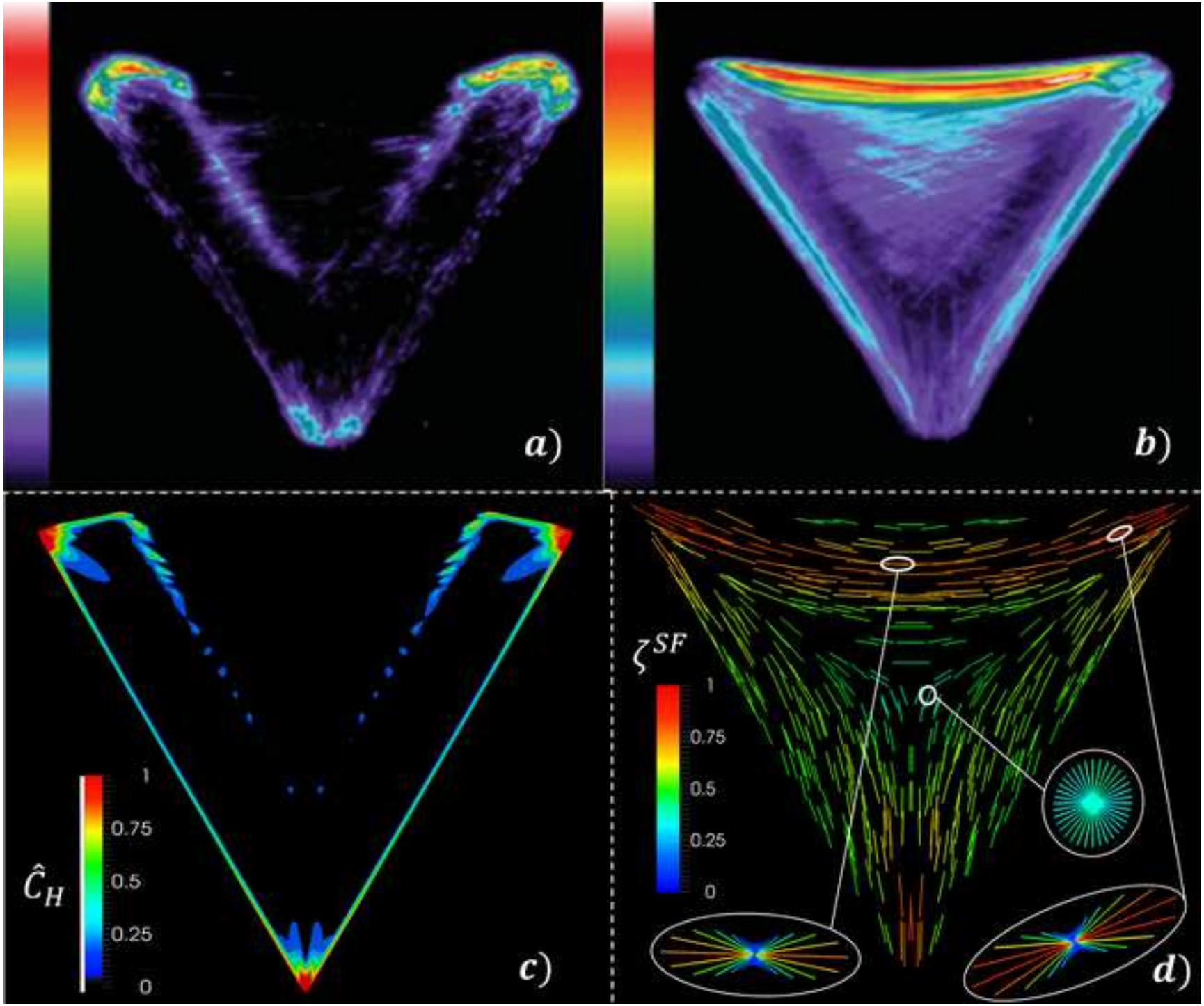

rev_fig10.tif

Click here to download high resolution image

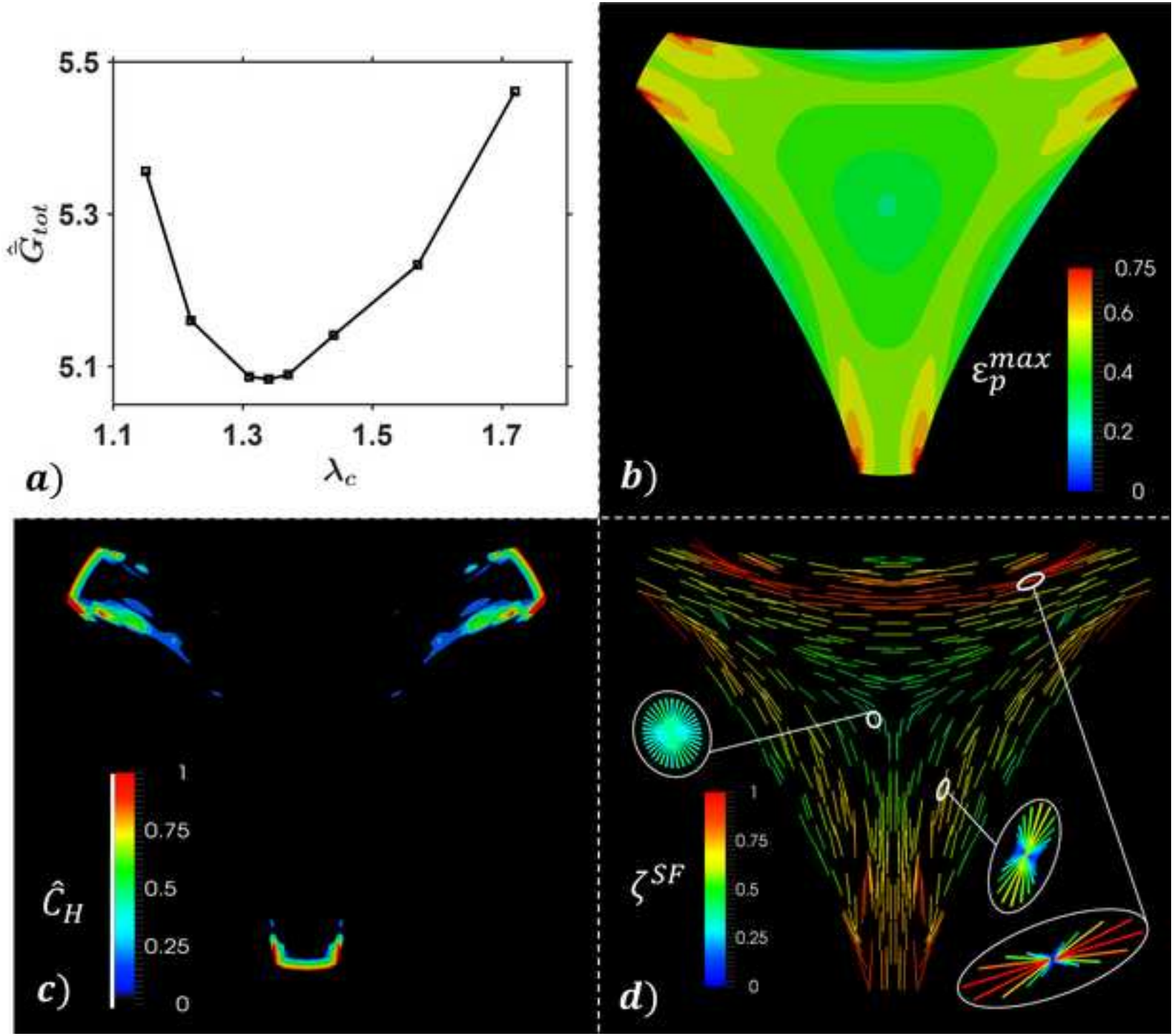

rev_fig11.tif
Click here to download high resolution image

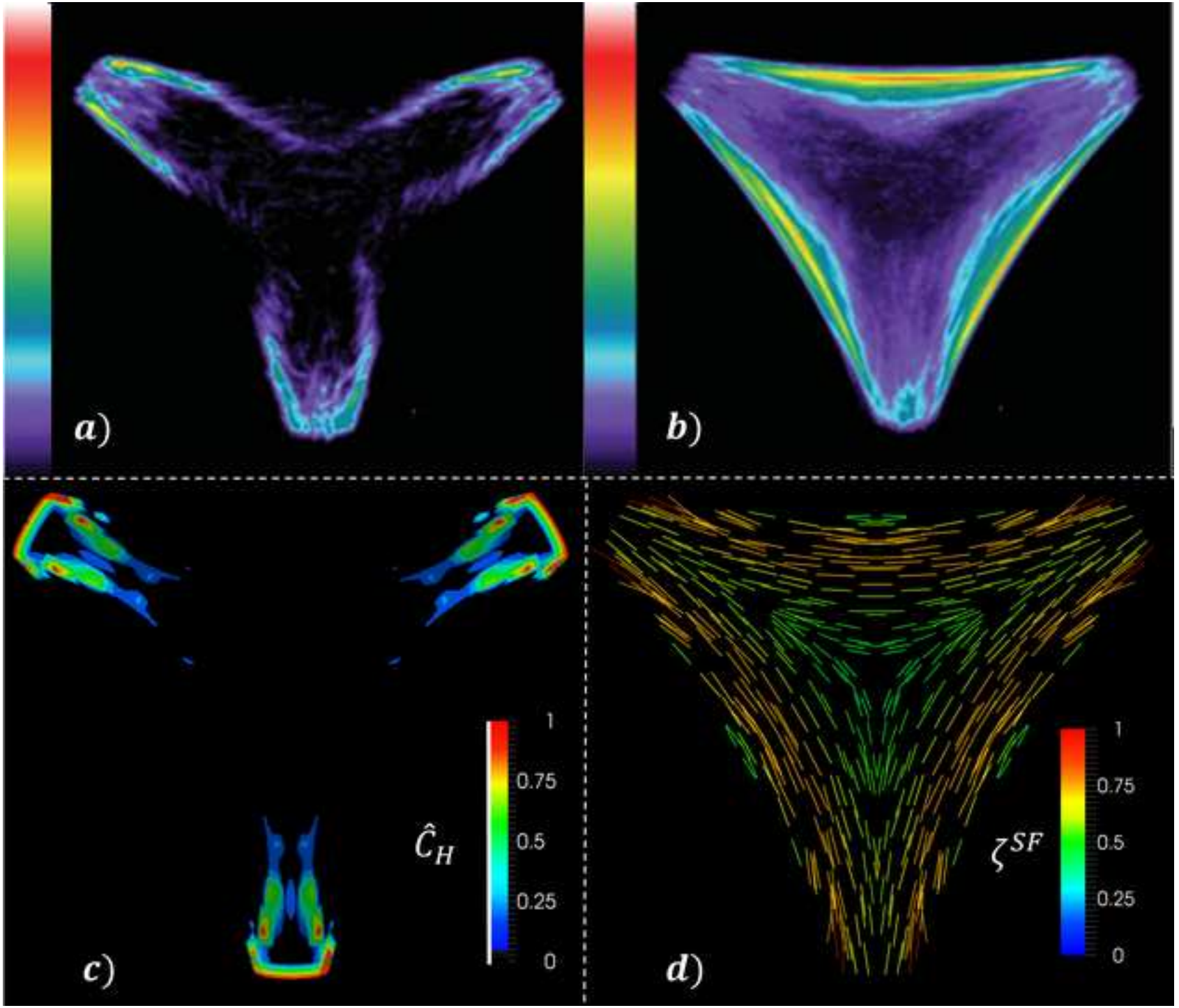

rev_figa_appendix.tif
Click here to download high resolution image